



Cite this: *Phys. Chem. Chem. Phys.*,  
2016, 18, 11610

Received 13th October 2015,  
Accepted 14th December 2015

DOI: 10.1039/c5cp06169e

www.rsc.org/pccp

## Endohedral Ca@B<sub>38</sub>: stabilization of a B<sub>38</sub><sup>2−</sup> borospherene dianion by metal encapsulation†

Qiang Chen,<sup>ab</sup> Hai-Ru Li,<sup>b</sup> Chang-Qing Miao,<sup>a</sup> Ying-Jin Wang,<sup>ab</sup> Hai-Gang Lu,<sup>b</sup> Yue-Wen Mu,<sup>b</sup> Guang-Ming Ren,<sup>\*a</sup> Hua-Jin Zhai<sup>\*bc</sup> and Si-Dian Li<sup>\*b</sup>

**Based on extensive global-minimum searches and first-principles electronic structure calculations, we present the viability of an endohedral metalloborospherene C<sub>s</sub> Ca@B<sub>38</sub> (1) which contains a C<sub>s</sub> B<sub>38</sub><sup>2−</sup> (2) dianion composed of interwoven boron double chains with a  $\sigma + \pi$  double delocalization bonding pattern, extending the B<sub>n</sub><sup>q</sup> (q = n − 40) borospherene family from n = 39–42 to n = 38. Transition metal endohedral complexes C<sub>s</sub> M@B<sub>38</sub> (M = Sc, Y, Ti) (3, 5, 7) based on C<sub>s</sub> B<sub>38</sub><sup>2−</sup> (2) are also predicted.**

As an electron-deficient element, boron has a strong propensity to form polyhedral structures with multicenter chemical bonding. However, gas-phase B<sub>n</sub><sup>−/0</sup> clusters have proved to be planar or quasi-planar in a wide range of sizes (n = 3–25, 27, 30, 35, 36),<sup>1–10</sup> in stark contrast to bulk boron. The possibility of all-boron fullerenes was not considered prior to the 2007 proposal of B<sub>80</sub> fullerene,<sup>11</sup> which is constructed from C<sub>60</sub> by capping the 20 surface hexagons. Subsequent computational investigations, however, showed that B<sub>80</sub> strongly favors the core-shell-type structures.<sup>12,13</sup> The first all-boron fullerenes D<sub>2d</sub> B<sub>40</sub><sup>−</sup> and B<sub>40</sub>, referred to as borospherenes in the literature, were discovered in 2014 by Zhai *et al.* in a combined experimental and theoretical study.<sup>14</sup> The first axially chiral borospherenes C<sub>3</sub>/C<sub>2</sub> B<sub>39</sub><sup>−</sup> were observed by Chen *et al.* in 2015.<sup>15</sup> Two cationic chiral members C<sub>1</sub> B<sub>41</sub><sup>+</sup> and C<sub>2</sub> B<sub>42</sub><sup>2+</sup> were recently introduced to the borospherene family by Chen *et al.* on the basis of global minimum (GM) structural searches.<sup>16</sup> The borospherenes B<sub>39</sub><sup>−</sup>, B<sub>40</sub>, B<sub>41</sub><sup>+</sup>, and B<sub>42</sub><sup>2+</sup> reported so far form a  $\pi$ -isovalent B<sub>n</sub><sup>q</sup> series in different charge states (q = n − 40). They are all composed of twelve interwoven boron double-chains (BDCs) with six hexagonal or heptagonal faces, that is, n<sub>6</sub> + n<sub>7</sub> = 6 with (n<sub>6</sub>, n<sub>7</sub>) = (3, 3), (2, 4), (1, 5), and (0, 6) for n = 39, 40, 41, and 42, respectively. Such “cubic-box-like”

borospherenes can be viewed as boron analogues of cubane (C<sub>8</sub>H<sub>8</sub>).<sup>14–16</sup> These borospherenes possess a universal bonding pattern of  $\sigma + \pi$  double delocalization, with 12 multicenter two-electron (mc-2e)  $\pi$ -bonds over a  $\sigma$ -skeleton with (n + 8) three-center two-electron (3c-2e)  $\sigma$ -bonds.<sup>14–16</sup>

The observations of D<sub>2d</sub> B<sub>40</sub><sup>−/0</sup> and C<sub>3</sub>/C<sub>2</sub> B<sub>39</sub><sup>−</sup> lead to a surge of research activities in borospherene chemistry, which is expected to parallel that of the fullerenes. Endohedral metalloborospherenes M@B<sub>40</sub> (M = Ca, Sr) were firstly predicted by Bai *et al.* at the density functional theory (DFT) level.<sup>17</sup> A computational study on the electronic structure and electronic spectra of D<sub>2d</sub> B<sub>40</sub>,<sup>18</sup> a topological analysis of D<sub>2d</sub> B<sub>40</sub>,<sup>19</sup> a theoretical study on endohedral M@B<sub>40</sub> (M = Sc, Y, La),<sup>20</sup> a molecular dynamics study on D<sub>2d</sub> B<sub>40</sub> “nanobubble” at high temperatures (1000 and 1200 K),<sup>21</sup> a theoretical prediction of the hydrogen-storage capacity of B<sub>40</sub>,<sup>22</sup> and a computational design of Au–B<sub>40</sub>–Au rectifier and photo-detector<sup>23</sup> quickly followed. Very recently, Chen *et al.* predicted the first axially chiral endohedral Ca@B<sub>39</sub><sup>+</sup> monocation, in which the B<sub>39</sub> cage serves as a superhalogen.<sup>24</sup> Borospherenes (B<sub>39</sub><sup>−</sup>, B<sub>40</sub>, B<sub>41</sub><sup>+</sup>, and B<sub>42</sub><sup>2+</sup>) possess the suitable cavities with a diameter of about 6.0 Å, which can host various kinds of alkaline earth and transition metals to form stable endohedral metalloborospherenes, similar to the well-known endohedral metallofullerenes: M@C<sub>60</sub> (M = La, Ca) and M@C<sub>76</sub> (M = Ca, Sr, Sm, Yb).<sup>25–32</sup> Borospherenes are also capable of forming stable exohedral metalloborospherenes on the surface heptagons, such as the recently predicted M&B<sub>40</sub> (M = Be, Mg).<sup>17</sup> Concerning smaller fullerene-like boron clusters, a high-symmetry D<sub>2h</sub> B<sub>38</sub> cage was recently predicted to be the lowest-lying isomer at the DFT level.<sup>33,34</sup> Based on D<sub>2h</sub> B<sub>38</sub>, a series of endohedral complexes M@B<sub>38</sub> (M = Sc, Y, Ti) were subsequently proposed by encapsulating a transition metal atom inside the D<sub>2h</sub> B<sub>38</sub> cage.<sup>35</sup> Note that the D<sub>2h</sub> B<sub>38</sub> cage possesses four hexagon holes as well as two capped hexagons. This structural pattern is basically different from the B<sub>n</sub><sup>q</sup> borospherene series (B<sub>39</sub><sup>−</sup>, B<sub>40</sub>, B<sub>41</sub><sup>+</sup>, and B<sub>42</sub><sup>2+</sup>) which are composed of interwoven BDCs with six hexagon/heptagon holes (but without capped hexagons).<sup>14–16</sup> Moreover, endohedral M@B<sub>40</sub> (M = Ca, Sr) and M@B<sub>38</sub> (M = Sc, Y, Ti) clusters involve electron

<sup>a</sup> Institute of Materials Science and Department of Chemistry, Xinzhou Teachers' University, Xinzhou 034000, China. E-mail: rgm\_xztc@126.com

<sup>b</sup> Nanocluster Laboratory, Institute of Molecular Science, Shanxi University, Taiyuan 030006, China. E-mail: hj.zhai@sxu.edu.cn, lisidian@sxu.edu.cn

<sup>c</sup> State Key Laboratory of Quantum Optics and Quantum Optics Devices, Shanxi University, Taiyuan 030006, China

† Electronic supplementary information (ESI) available. See DOI: 10.1039/c5cp06169e

donation from the metal centers to the high-lying LUMOs of  $D_{2d}$   $B_{40}$  and  $D_{2h}$   $B_{38}$  cages which have huge HOMO–LUMO gaps.<sup>14,33</sup> Such orbital occupations should destabilize the endohedral systems thermodynamically. On the other hand, for neutral  $B_n$  cages with  $n < 40$  which lack the necessary valence electrons to match the  $\sigma + \pi$  double delocalization bonding pattern for stable borospherenes, metal encapsulation is anticipated to help stabilize the systems. The current work represents an exploration in this direction.

Based on extensive GM searches and first-principles calculations, we present herein the possibility of the neutral endohedral  $C_s$   $Ca@B_{38}$  (**1**) which is composed of twelve interwoven BDCs with a  $\sigma + \pi$  double delocalization bonding pattern.  $Ca@B_{38}$  (**1**) is a charge-transfer complex  $Ca^{2+}@B_{38}^{2-}$  which contains a  $C_s$   $B_{38}^{2-}$  (**2**) borospherene dianion effectively stabilized by a  $Ca^{2+}$  dication encapsulated inside. The infrared (IR) and Raman spectra of **1** as well as the photoelectron spectra of two  $C_s$   $Ca@B_{38}^-$  monoanions corresponding to the two lowest-lying isomers of  $CaB_{38}$  are simulated, which should facilitate their forthcoming experimental characterization. Transition metal endohedral  $C_s$   $M@B_{38}$  ( $M = Sc, Y,$  and  $Ti$ ) based on  $C_s$   $B_{38}^{2-}$  (**2**) are also predicted which turn out to be far more stable than the recently proposed  $C_{2v}$   $M@B_{38}$  endohedral clusters<sup>35</sup> based on  $D_{2h}$   $B_{38}$ .<sup>33,34</sup>

Global structural searches were performed for  $CaB_{38}$  using the minima hopping (MH) algorithm<sup>13,36</sup> at DFT, in combination with manual structural constructions based on the typical planar, cage-like, and tubular isomers of  $B_{38}$ .<sup>33,34,37</sup> Low-lying isomers were then fully optimized with frequencies checked and their relative energies evaluated at the hybrid DFT-PBE0<sup>38</sup> level with the 6-311+G(d) basis set<sup>39</sup> as implemented in the Gaussian 09 suite.<sup>40</sup> The Stuttgart relativistic small-core pseudopotential and valence basis sets<sup>41,42</sup> were used for Sr and Y. Relative stabilities of the low-lying isomers within 0.5 eV were further refined using the coupled cluster method with triple excitations (CCSD(T))<sup>43–45</sup> implemented in MOLPRO<sup>46</sup> with the 6-311G(d) basis set at PBE0 geometries. Molecular dynamics (MD) simulations were performed for the two lowest-lying isomers of  $CaB_{38}$  at 200, 300, and 500 K for 30 ps using the CP2K suite.<sup>47</sup> The optimized structure of endohedral  $Ca@B_{38}$  (**1**) compared with that of the  $B_{38}^{2-}$  (**2**) dianion is depicted in Fig. 1. Alternative isomeric structures are summarized in Fig. S1 for  $CaB_{38}$  in the ESI.† Fig. 2 shows the configuration energy spectrum of  $CaB_{38}$  at PBE0. Fig. 3 presents the bonding patterns of the two lowest-lying isomers of  $Ca@B_{38}$  using the adaptive natural density partitioning (AdNDP) method,<sup>48</sup> which includes

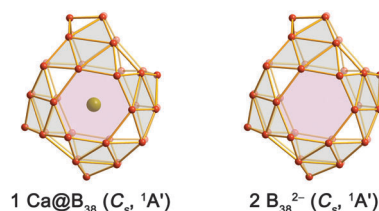


Fig. 1 Optimized structure of  $C_s$   $Ca@B_{38}$  (**1**) compared with that of  $C_s$   $B_{38}^{2-}$  (**2**) at the PBE0/6-311+G(d) level. The eight almost perfectly planar, close-packed  $B_6$  triangles at the corners of the cubic-box are shaded in grey.

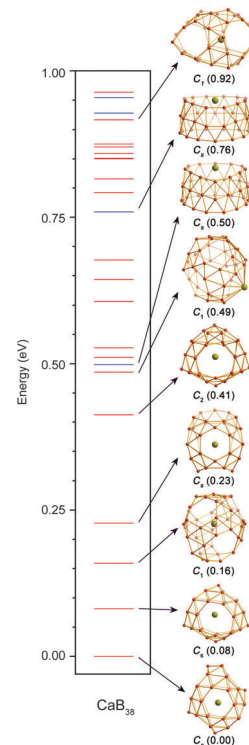


Fig. 2 Configurational energy spectrum of  $CaB_{38}$  at PBE0/6-311+G(d), with the relative energies indicated in eV. The red and blue bars denote cage-like structures and triple-ring tubes, respectively.

the mc-2e bonding elements. Fig. 4 depicts the simulated photoelectron spectra of two  $C_s$   $Ca@B_{38}^-$  monoanions which correspond to the two lowest-lying isomers of  $CaB_{38}$  (Fig. 2), using the time-dependent DFT (TD-PBE0) approach.<sup>49</sup> Fig. 5 shows the optimized structures of endohedral  $C_s$   $M@B_{38}$  ( $M = Sc, Y,$  and  $Ti$ ) (**3, 5, 7**), compared with their  $C_{2v}$   $M@B_{38}$  counterparts (**4, 6, 8**).

Considering the fact that high-symmetry cage-like  $D_{2h}$   $B_{38}$  has been predicted to be the lowest-energy isomer of  $B_{38}$  at PBE0,<sup>33</sup> it is reasonable to anticipate that the endohedral  $D_{2h}$   $Ca@B_{38}$  cluster be energetically favorable for  $CaB_{38}$ . However, as clearly indicated in Fig. S1 in the ESI,† our MH global searches, with more than 2800 stationary points being probed

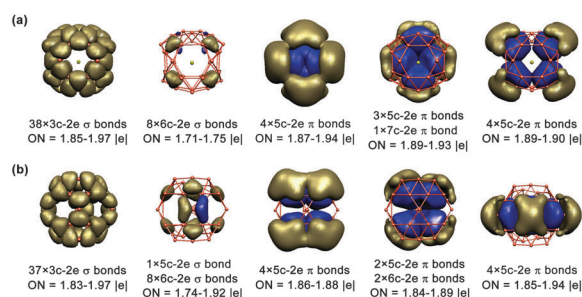


Fig. 3 The AdNDP bonding patterns of (a) the global minimum  $CaB_{38}$  (**1**) and (b) the second lowest-lying isomer  $CaB_{38}$ , with the occupation numbers (ONs) indicated. Both structures are rotated with respect to the original orientations in Fig. 1 and 2 to make their mirror planes perpendicular to the paper surface.

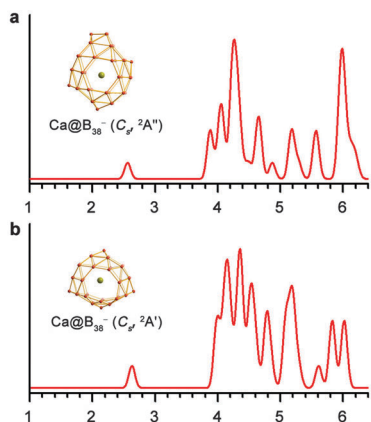


Fig. 4 Simulated photoelectron spectra of (a)  $C_s$   $\text{Ca@B}_{38}^-$  (**1**) and (b)  $C_s$   $\text{Ca@B}_{38}^-$  which correspond to the global minimum and the second lowest-lying isomer of  $\text{CaB}_{38}$  shown in Fig. 2, respectively.

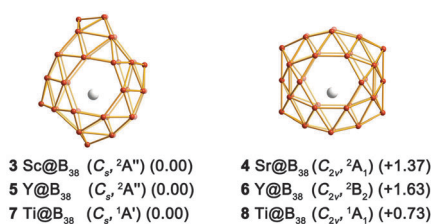


Fig. 5 Optimized endohedral  $C_s$   $\text{M@B}_{38}$  ( $M = \text{Sc}, \text{Y}, \text{Ti}$ ) (**3**, **5**, and **7**) compared with the recently proposed  $C_{2v}$   $\text{M@B}_{38}$  ( $M = \text{Sc}, \text{Y}, \text{Ti}$ ) (**4**, **6**, and **8**), with their relative energies indicated in eV at the PBE0 level. High symmetry structures are depicted for comparison and clarity.

on the potential energy surface, show that a dramatic structural change occurs from  $\text{B}_{38}$  to  $\text{CaB}_{38}$ : the endohedral  $C_s$   $\text{Ca@B}_{38}$  (**1**,  $^1A'$ ) turns out to be the GM of the  $\text{CaB}_{38}$  complex, which possesses a  $C_s$   $\text{B}_{38}$  cage composed of twelve interwoven BDCs with four hexagonal and two heptagonal faces, that is  $(n_6, n_7) = (4, 2)$ . In contrast, the endohedral  $D_{2h}$   $\text{Ca@B}_{38}$  based on the  $D_{2h}$   $\text{Ca@B}_{38}$  cage motif is much less stable (by 1.47 eV; Fig. S1 in the ESI†) than the GM, mainly due to the fact that it involves an electron transfer from the Ca center to the high-lying LUMO (2.25 eV above the HOMO) of the  $D_{2h}$   $\text{B}_{38}$  cage.<sup>33</sup>

Interestingly,  $C_s$   $\text{Ca@B}_{38}$  (**1**) possesses a  $C_s$   $\text{B}_{38}$  cage motif, which follows the structural pattern of the borospherene family. The  $C_s$   $\text{B}_{38}$  cage can be obtained by replacing two neighboring  $B_7$  heptagons on the waist of  $D_{2d}$   $\text{B}_{40}$  with two  $B_6$  hexagons,<sup>14</sup> or by replacing two neighboring hexagons on cage-like  $C_{2h}$   $\text{B}_{36}$  with two heptagons,<sup>9</sup> followed by a full structural optimization.  $\text{Ca@B}_{38}$  (**1**) looks like a filled “basket”, with two staggered heptagons on the top, two eclipsed hexagons in the middle, and two staggered hexagons at the bottom. It can also be viewed as a distorted cubic-box made of eight almost perfectly planar, close-packed  $B_6$  triangles at the eight corners (Fig. 1), similar to  $D_{2d}$   $\text{B}_{40}$ .<sup>14</sup> With 46  $B_3$  triangles, four  $B_6$  hexagons, and two  $B_7$  heptagons on the surface,  $\text{Ca@B}_{38}$  (**1**) follows the Euler’s rule:  $E$  (88 edges) =  $F$  (46 triangular + 4 hexagonal + 2 heptagonal faces) +  $V$  (38 vertices) – 2. As detailed below, **1** is a charge-transfer complex in nature,  $\text{Ca}^{2+}@\text{B}_{38}^{2-}$ ,

which follows the universal bonding pattern of  $\sigma + \pi$  double delocalization for stable borospherenes. Here the  $\text{B}_{38}^{2-}$  dianion cage is effectively stabilized by the  $\text{Ca}^{2+}$  dication encapsulated inside, mainly *via* the electrostatic effect.  $\text{Ca@B}_{38}$  (**1**) represents the first neutral endohedral metalloborospherene with a  $C_s$   $\text{B}_{38}^{2-}$  shell (**2**).

The second lowest-lying isomer  $C_s$   $\text{Ca@B}_{38}$  ( $^1A'$ ), which contains three hexagons and three heptagons ( $(n_6, n_7) = (3, 3)$ ), lies very close in energy to the GM (by 0.08 eV at PBE0; Fig. 2). It possesses a  $C_s$   $\text{B}_{38}$  cage that can be achieved by replacing one  $B_7$  heptagon on  $D_{2d}$   $\text{B}_{40}$  with a  $B_6$  hexagon and removing one B atom from a BDC to form a tetracoordinate B “defect” site between two neighboring hexagons on the mirror surface, similar to the experimentally observed  $C_2$   $\text{B}_{39}^-$ .<sup>15</sup> At the more accurate CCSD(T) level, the relative energy between these two isomers is only 0.03 eV, indicating that they are practically isoenergetic isomers and may coexist in experiments.

The third lowest-lying isomer  $C_1$   $\text{Ca@B}_{38}$  ( $^1A$ ) is 0.16 eV above the GM at PBE0. It also contains three hexagons and three heptagons, that is  $(n_6, n_7) = (3, 3)$ , which can be obtained from the experimentally observed  $C_3$   $\text{B}_{39}^-$  (ref. 15) by removing one B atom from a BDC between two neighboring heptagons to form a tetracoordinate B site. The fourth isomer  $C_s$   $\text{Ca@B}_{38}$  ( $^1A$ ) lies 0.23 eV higher than the GM, with two neighboring hexagons and four heptagons ( $(n_6, n_7) = (2, 4)$ ). It can be achieved by replacing one hexagon from  $C_3$   $\text{B}_{39}^-$  ref. 15 with a heptagon, with one heptagon on the mirror surface possessing two tetracoordinate B sites on opposite sides. The fifth isomer  $C_2$   $\text{Ca@B}_{38}$  ( $^1A$ ) lies 0.41 eV above the GM. It also possesses two hexagons and four heptagons ( $(n_6, n_7) = (2, 4)$ ), with two tetracoordinate B sites at the two ends of the  $C_2$  axis. The sixth isomer  $C_1$   $\text{Ca@B}_{38}$  ( $^1A$ ) with a relative energy of 0.49 eV is the first exohedral isomer, with the Ca atom capping a  $B_9$  ring. The seventh isomer  $C_s$   $\text{Ca@B}_{38}$  ( $^1A$ ) is a capped triple-ring tube, being 0.50 eV higher than the GM. At the more reliable CCSD(T) level, the third to seventh isomers are 0.06, 0.09, 0.18, 0.22, and 0.40 eV higher than the GM, respectively, well supporting the energetics at PBE0. The first quasi-planar  $C_s$   $\text{CaB}_{38}$  ( $^1A$ ) with a Ca-capped  $B_8$  octagon lies 1.36 eV higher than the GM at PBE0 (Fig. S1 in the ESI†). Note that all the five lowest-lying isomers of  $\text{CaB}_{38}$  possess endohedral geometries, which are the most possible candidates to be synthesized in experiments. Preliminary investigations at PBE0 also indicate that both endohedral  $C_s$   $\text{Mg@B}_{38}$  and  $C_s$   $\text{Sr@B}_{38}$  based on  $C_s$   $\text{B}_{38}^{2-}$  (**2**) are a true minimum of the systems, with the former favoring an exohedral  $C_1$   $\text{Mg@B}_{38}$  (similar to the sixth isomer of  $\text{CaB}_{38}$  in Fig. 2) by 0.75 eV and the latter favoring a capped triple-ring tubular  $C_s$   $\text{Sr@B}_{38}$  (similar to the seventh isomer of  $\text{CaB}_{38}$ ) by 0.12 eV, respectively, possibly due to size effects in the alkaline earth metal series.<sup>17</sup>

The stabilities of the two lowest-lying  $\text{CaB}_{38}$  isomers are further explored using the MD simulations. As shown in Fig. S2 in the ESI†,  $\text{Ca@B}_{38}$  (**1**) is dynamically stable at 200, 300, and 500 K, with the root-mean-square-deviations of RMSD = 0.06, 0.07, and 0.10 Å and the maximum bond length deviations of MAXD = 0.20, 0.24, and 0.36 Å (on average), respectively

(Fig. S2a, ESI<sup>†</sup>). The second  $C_s$  isomer is also stable at both 200 and 300 K with RMSD = 0.06 and 0.08 Å and MAXD = 0.22 and 0.27 Å, respectively. However, it starts to fluctuate between two equivalent  $C_s$  isomers at 500 K with RMSD = 0.13 Å and MAXD = 0.56 Å (Fig. S2b, ESI<sup>†</sup>). Interestingly, the two  $C_s$  isomers are interlinked *via* a  $C_2$  intermediate structure in a concerted mechanism, which contains a tetracoordinate B site between two neighboring heptagons on the  $C_2$  axis (Fig. S2c, ESI<sup>†</sup>). Further simulations indicate that  $\text{Ca@B}_{38}$  (**1**) also “hops” at 700 K between the three lowest-lying isomers of  $\text{CaB}_{38}$  (Fig. 2). The MD behaviors reflect the glassy nature of nanoboron at high temperatures.<sup>15,16,21,24</sup>

Endohedral metalloborospherenes  $C_s$   $\text{Ca@B}_{38}$  (**1**) and the second lowest-lying  $C_s$   $\text{Ca@B}_{38}$  possess unique electronic structures and bonding patterns. Indeed, they have the large HOMO–LUMO gaps of 2.70 eV and 2.58 eV at PBE0 (Fig. S3, ESI<sup>†</sup>), respectively, comparable with the corresponding values of 2.89, 2.73, and 3.13 eV obtained for  $C_3$   $\text{B}_{39}^-$ ,  $C_2$   $\text{B}_{39}^-$ , and  $D_{2d}$   $\text{B}_{40}$  at the same level.<sup>14,15</sup> Natural bonding orbital (NBO) analyses show that the Ca centers in these complexes carry the positive charges of +1.69  $|e|$  and 1.71  $|e|$ , respectively, with the electronic configurations of  $[\text{Ar}]4s^{0.12}3d^{0.17}$  and  $[\text{Ar}]4s^{0.12}3d^{0.16}$ . These results clearly indicate that the Ca center in these complexes donates two  $4s^2$  electrons to the  $C_s$   $\text{B}_{38}$  cage, which behaves like a superoxygen (similar to  $\text{B}_{39}$  which serves as a superhalogen in  $\text{Ca@B}_{39}^+$  (ref. 24)). These charge-transfer complexes mainly exhibit ionic interactions between the  $\text{Ca}^{2+}$  dication center and the  $\text{B}_{38}^{2-}$  dianion shell. Weak back donations from the  $\pi$  orbitals of  $\text{B}_{38}^{2-}$  (as analyzed below) to the empty 4d orbitals of Ca may also contribute to the stabilization of the complexes. The calculated formation energies of  $\Delta E_f = -127.7$  and  $\Delta E_f = -131.9$  kcal mol<sup>-1</sup> with respect to  $\text{B}_{38}(\text{C}_s) + \text{Ca} = \text{Ca@B}_{38}(\text{C}_s)$  and the vertical ionization potentials of 7.35 and 7.16 eV further demonstrate the thermodynamic stability of these neutral complexes.

The AdNDP analyses reveal the bonding pattern of complex  $C_s$   $\text{CaB}_{38}$  (**1**) and its second lowest-lying isomer. As shown in Fig. 3a, **1** possesses 38 3c-2e  $\sigma$  bonds on 38  $\text{B}_3$  triangles, as well as 8 6c-2e  $\sigma$  bonds on 8  $\text{B}_6$  triangles on the cage surface. Since the central  $\text{B}_3$  triangles make major contribution to the 6c-2e  $\sigma$  bonds, the  $\sigma$  framework can be practically treated as 46 3c-2e  $\sigma$  bonds, evenly distributed on the cage surface with one  $\sigma$  bond per  $\text{B}_3$  triangle. The remaining 12 bonds form the  $\pi$  framework. It can be classified into three groups, with one 7c-2e  $\pi$  bond over the BDC between two neighboring heptagons and 11 5c-2e  $\pi$  bonds over the other 11 BDCs, which again cover the cage surface almost uniformly. Thus all 116 valence electrons in **1** participate in delocalized  $\sigma$  and  $\pi$  covalent bonds on the cage surface, following the established bonding pattern of  $\sigma + \pi$  double delocalization for borospherenes.<sup>14–16</sup> The second lowest-lying endohedral isomer  $C_s$   $\text{Ca@B}_{38}$  also features a similar bonding pattern, with 45 3c-2e  $\sigma$  bonds on  $\text{B}_3$  triangles and one 5c-2e  $\sigma$  bond at the tetracoordinate B site, as well as 12 5c-2e or 6c-2e  $\pi$  bonds (Fig. 3b). There exist no localized bonds in these complexes.

Note that a neutral  $C_s$   $\text{B}_{38}$  cage lacks two valence electrons to satisfy the  $\sigma + \pi$  double delocalization bonding requirement of

a borospherene; the Ca center in **1** donates exactly two  $4s^2$  electrons to compensate for this electron deficiency. The optimized  $C_s$   $\text{B}_{38}^{2-}$  dianion (**2**) is a true minimum with the smallest vibrational frequency of 160 cm<sup>-1</sup> and the HOMO–LUMO energy gap of 2.54 eV. It possesses exactly the same  $\sigma + \pi$  double delocalization bonding pattern as  $C_s$   $\text{CaB}_{38}$  (**1**) (Fig. 3a). It is also 3D aromatic with the highly negative nucleus-independent chemical shift (NICS)<sup>50</sup> of -37 ppm at the cage center, comparable to the corresponding value of NICS = -42 ppm of  $D_{2d}$   $\text{B}_{40}$ .<sup>14</sup> However,  $C_s$   $\text{B}_{38}^{2-}$  (**2**) is not the GM of the dianion due to strong intramolecular Coulomb repulsion in the cage structure. The Ca center in **1** serves as a dication that neutralizes the negative charge of the  $\text{B}_{38}^{2-}$  dianion cage carries, rendering high stability to **1** as the GM of the complex. Similar analyses apply to the second lowest-lying isomer of  $\text{CaB}_{38}$  in Fig. 2.

Anion photoelectron spectroscopy in combination with first-principles calculations has proved to be a powerful approach in characterizing nanoclusters in the gas phase.<sup>1–10,14,15</sup> We simulate the photoelectron spectra of the two  $C_s$   $\text{Ca@B}_{38}^-$  monoanions which correspond to the two lowest-lying isomers of  $\text{CaB}_{38}$  at PBE0 (Fig. 4) to aid their future experimental characterization. Remarkably, the two isomers possess similar photoelectron spectra with the experimentally observed  $D_{2d}$   $\text{B}_{40}^-$ .<sup>14</sup> The calculated first adiabatic and vertical detachment energies (ADE/VDE) of the two  $C_s$   $\text{Ca@B}_{38}^-$  isomers are 2.44/2.55 and 2.52/2.62 eV, respectively. Their calculated energy gaps amount to 1.32 and 1.35 eV. The sizable energy gaps of the two  $C_s$   $\text{Ca@B}_{38}^-$  monoanions are consistent with the electronic stability of their neutrals, which have large HOMO–LUMO gaps as presented above (Fig. S3, ESI<sup>†</sup>). In fact, both  $C_s$   $\text{Ca@B}_{38}$  (**1**) and the second lowest-lying  $C_s$   $\text{Ca@B}_{38}$  are  $\pi$ -isovalent with the observed  $D_{2d}$   $\text{B}_{40}$  borospherene. These neutral metalloborospherenes and their monoanions invite forthcoming experimental explorations.

Vibrational spectroscopy has also proved to be an effective approach for experimental studies of nanoclusters.<sup>51</sup> We calculate the vibrational frequencies and simulate the IR and Raman spectra of  $\text{Ca@B}_{38}$  (**1**) at PBE0 (Fig. S4 in the ESI<sup>†</sup>), which are compared with those of  $\text{B}_{38}^{2-}$  (**2**). The three major IR peaks at 1220 ( $a'$ ), 811 ( $a'$ ), and 416 ( $a''$ ) in **2** are basically maintained in **1**, with small blue shifts (Fig. S4a, ESI<sup>†</sup>). The main Raman features of **2** are also inherited in **1** (Fig. S4b, ESI<sup>†</sup>). The two  $a'$  breathing modes at 254 cm<sup>-1</sup> and 454 cm<sup>-1</sup> belong to “radial breathing modes” (RBMs) of the  $\text{B}_{38}^{2-}$  (**2**) cage. RBMs have been used to identify the hollow structures of the single-walled boron nanotubes.<sup>52</sup>

Finally, we brief the results obtained for the series of transition metal doped endohedral complexes:  $\text{M@B}_{38}$  ( $\text{M} = \text{Sc}, \text{Y}, \text{Ti}$ ). As shown in Fig. 5, the endohedral  $C_s$   $\text{Sc@B}_{38}$  (**3**),  $C_s$   $\text{Y@B}_{38}$  (**5**), and  $C_s$   $\text{Ti@B}_{38}$  (**7**) based on the  $C_s$   $\text{B}_{38}^{2-}$  (**2**) motif are 1.37, 1.63, and 0.73 eV more stable than the recently proposed  $C_{2v}$   $\text{Sc@B}_{38}$  (**4**),  $C_{2v}$   $\text{Y@B}_{38}$  (**6**), and  $C_{2v}$   $\text{Ti@B}_{38}$  (**8**)<sup>35</sup> based on the  $D_{2h}$   $\text{B}_{38}$  cage<sup>33</sup> at the PBE0 level, respectively. Such huge energy differences are in good agreement with the calculated encapsulation energies of -163.5, -114.5, -182.8, -127.8, -186.9, and -152.7 kcal mol<sup>-1</sup> for **3**, **4**, **5**, **6**, **7**, and **8**, respectively, and strongly suggest that **3**, **5**, and **7** be far more viable in experiments than **4**, **6**, and **8**. The NBO analyses show that the metal centers in **3**, **4**, **5**, **6**, **7**, and **8**

possess the natural atomic charges of +1.09, +0.80, +1.07, +1.15, +0.88, and +0.50  $|e|$ , respectively, indicating that the transition metal centers donate valence electrons to the cage-like  $B_{38}$  ligands, in line with the fact that boron has a higher electronegativity (2.04 in the Pauling scale) than all the transition metals Sc(1.36), Y(1.22), and Ti(1.54) concerned in this work. The high stabilities of **3**, **5**, and **7** over **4**, **6**, and **8** can be understood based on the fact that the cage-like  $C_s B_{38}$  ligand requires extra electrons from the metal center to satisfy the bonding pattern of a stable borospherene while  $D_{2h} B_{38}$  possesses a stable closed-shell electronic configuration with a huge HOMO–LUMO gap of 2.25 eV.<sup>33</sup> There exist also obvious  $\pi \rightarrow d$  back donations from the  $B_{38}$  ligands to the transition metal centers in these complexes, as demonstrated by the electron configurations of Sc  $[Ar]4s^{0.16}3d^{1.75}$ , Y  $[Kr]5s^{0.20}4d^{1.30}$ , and Ti  $[Ar]4s^{0.15}3d^{2.97}$  in **3**, **5**, and **7**, respectively. We stress here that the current prediction of **3**, **5**, and **7** testifies to the idea of computational design of novel boron nanostructures on the basis of the structural principles and bonding patterns of borospherenes.

In conclusion, we have presented the viability of the endohedral metalloborospherene  $Ca@B_{38}$  (**1**) via extensive global structural searches, first-principles calculations, and bonding analyses.  $Ca@B_{38}$  (**1**) contains a  $B_{38}^{2-}$  (**2**) borospherene shell, which is stabilized by the encapsulation of a  $Ca^{2+}$  center, forming the charge-transfer complex  $Ca^{2+}@B_{38}^{2-}$ . The complex is composed of twelve interwoven BDCs with six hexagonal/heptagonal faces which satisfy the bonding pattern of  $\sigma + \pi$  double delocalization for borospherenes. Similar transition-metal-doped endohedral metalloborospherenes  $C_s M@B_{38}$  (**3**, **5**, **7**) are also predicted computationally, which turn out to be far more stable than the previously proposed  $C_{2v} M@B_{38}$  clusters (**4**, **6**, **8**). The results achieved in this work suggest vast opportunities for rational design of novel boron nanostructures using the structural and bonding patterns of borospherenes.

## Acknowledgements

This work was supported by the National Natural Science Foundation of China (21373130, 21573138), the Key Research Project of Xinzhou Teachers' University (XK201303), and the State Key Laboratory of Quantum Optics and Quantum Optics Devices (KF201402). H. J. Z. gratefully acknowledges the start-up fund from Shanxi University for support.

## Notes and references

- H. J. Zhai, A. N. Alexandrova, K. A. Birch, A. I. Boldyrev and L. S. Wang, *Angew. Chem., Int. Ed.*, 2003, **42**, 6004–6008.
- H. J. Zhai, B. Kiran, J. Li and L. S. Wang, *Nat. Mater.*, 2003, **2**, 827–833.
- B. Kiran, S. Bulusu, H. J. Zhai, S. Yoo, X. C. Zeng and L. S. Wang, *Proc. Natl. Acad. Sci. U. S. A.*, 2005, **102**, 961–964.
- W. Huang, A. P. Sergeeva, H. J. Zhai, B. B. Averkiev, L. S. Wang and A. I. Boldyrev, *Nat. Chem.*, 2010, **2**, 202–206.
- E. Oger, N. R. M. Crawford, R. Kelting, P. Weis, M. M. Kappes and R. Ahlrichs, *Angew. Chem., Int. Ed.*, 2007, **46**, 8503–8506.
- W. L. Li, Y. F. Zhao, H. S. Hu, J. Li and L. S. Wang, *Angew. Chem., Int. Ed.*, 2014, **53**, 5540–5545.
- W. L. Li, Q. Chen, W. J. Tian, H. Bai, Y. F. Zhao, H. S. Hu, J. Li, H. J. Zhai, S. D. Li and L. S. Wang, *J. Am. Chem. Soc.*, 2014, **136**, 12257–12260.
- Z. A. Piazza, H. S. Hu, W. L. Li, Y. F. Zhao, J. Li and L. S. Wang, *Nat. Commun.*, 2014, **5**, 3113.
- Q. Chen, G. F. Wei, W. J. Tian, H. Bai, Z. P. Liu, H. J. Zhai and S. D. Li, *Phys. Chem. Chem. Phys.*, 2014, **16**, 18282–18287.
- (a) A. N. Alexandrova, A. I. Boldyrev, H. J. Zhai and L. S. Wang, *Coord. Chem. Rev.*, 2006, **250**, 2811–2866; (b) C. Romanescu, T. R. Galeev, W. L. Li, A. I. Boldyrev and L. S. Wang, *Acc. Chem. Res.*, 2013, **46**, 350–358; (c) A. P. Sergeeva, I. A. Popov, Z. A. Piazza, W. L. Li, C. Romanescu, L. S. Wang and A. I. Boldyrev, *Acc. Chem. Res.*, 2014, **47**, 1349–1358.
- N. G. Szwacki, A. Sadrzadeh and B. I. Yakobson, *Phys. Rev. Lett.*, 2007, **98**, 166804.
- F. Li, P. Jin, D.-E. Jiang, L. Wang, S. Zhang, J. Zhao and Z. Chen, *J. Chem. Phys.*, 2012, **136**, 074302.
- S. De, A. Willand, M. Amsler, P. Pochet, L. Genovese and S. Goedecker, *Phys. Rev. Lett.*, 2011, **106**, 225502.
- H. J. Zhai, Y. F. Zhao, W. L. Li, Q. Chen, H. Bai, H. S. Hu, Z. A. Piazza, W. J. Tian, H. G. Lu, Y. B. Wu, Y. W. Mu, G. F. Wei, Z. P. Liu, J. Li, S. D. Li and L. S. Wang, *Nat. Chem.*, 2014, **6**, 727–731.
- Q. Chen, W. L. Li, Y. F. Zhao, S. Y. Zhang, H. S. Hu, H. Bai, H. R. Li, W. J. Tian, H. G. Lu, H. J. Zhai, S. D. Li, J. Li and L. S. Wang, *ACS Nano*, 2015, **9**, 754–760.
- Q. Chen, S. Y. Zhang, H. Bai, W. J. Tian, T. Gao, H. R. Li, C. Q. Miao, Y. W. Mu, H. G. Lu, H. J. Zhai and S. D. Li, *Angew. Chem., Int. Ed.*, 2015, **54**, 8160–8164.
- H. Bai, Q. Chen, H. J. Zhai and S. D. Li, *Angew. Chem., Int. Ed.*, 2014, **54**, 941–945.
- R. X. He and X. C. Zeng, *Chem. Commun.*, 2015, **51**, 3185–3188.
- P. Schwerdtfeger, L. N. Wirz and J. Avery, *WIREs Comput. Mol. Sci.*, 2015, **5**, 96–145.
- P. Jin, Q. Hou, C. Tang and Z. Chen, *Theor. Chem. Acc.*, 2015, **134**, 13–22.
- G. Martínez-Guajardo, J. L. Cabellos, A. Díaz-Celaya, S. Pan, R. Islas, P. K. Chattaraj, T. Heine and G. Merino, *Sci. Rep.*, 2015, **5**, 11287.
- H. Dong, T. Hou, S. T. Lee and Y. Li, *Sci. Rep.*, 2015, **5**, 09952.
- Z. Yang, Y. L. Ji, G. Lan, L. C. Xu, X. Liu and B. Xu, *Solid State Commun.*, 2015, **217**, 38–42.
- Q. Chen, T. Gao, W. J. Tian, H. Bai, S. Y. Zhang, H. R. Li, C. Q. Miao, Y. W. Mu, H. G. Lu, H. J. Zhai and S. D. Li, *Phys. Chem. Chem. Phys.*, 2015, **17**, 19690–19694.
- J. R. Heath, S. C. O'Brien, Q. Zhang, Y. Liu, R. F. Curl, H. W. Kroto, F. K. Tittel and R. E. Smalley, *J. Am. Chem. Soc.*, 1985, **107**, 7779–7780.
- Z. Wan, J. F. Christian and S. L. Anderson, *Phys. Rev. Lett.*, 1992, **69**, 1352–1355.
- P. Weis, R. D. Beck, G. Bräuchle and M. M. Kappes, *J. Chem. Phys.*, 1994, **100**, 5684–5695.
- Y. Kubozono, H. Maeda, Y. Takabayashi, K. Hiraoka, T. Nakai, S. Kashino, S. Emura, S. Ukita and T. Sogabe, *J. Am. Chem. Soc.*, 1996, **118**, 6998–6999.

- 29 L. S. Wang, J. M. Alford, Y. Chai, M. Diener, J. Zhang, S. M. McClure, T. Guo, G. E. Scuseria and R. E. Smalley, *Chem. Phys. Lett.*, 1993, **207**, 354–359.
- 30 M. Saunders, R. J. Cross, H. A. Jiménez-Vázquez, R. Shimshi and A. Khong, *Science*, 1996, **271**, 1693–1697.
- 31 T. A. Murphy, T. Pawlik, A. Weidinger, M. Höhne, R. Alcalá and J. M. Spaeth, *Phys. Rev. Lett.*, 1996, **77**, 1075–1078.
- 32 J. Lu, X. W. Zhang and X. G. Zhao, *Chem. Phys. Lett.*, 1999, **312**, 85–90.
- 33 J. Lv, Y. Wang, L. Zhu and Y. Ma, *Nanoscale*, 2014, **6**, 11692–11696.
- 34 T. B. Tai and M. T. Nguyen, *Nanoscale*, 2015, **7**, 3316–3317.
- 35 Q. L. Lu, Q. Q. Luo, Y. D. Li and S. G. Huang, *Phys. Chem. Chem. Phys.*, 2015, **17**, 20897–20902.
- 36 S. Goedecker, W. Hellmann and T. Lenosky, *Phys. Rev. Lett.*, 2005, **95**, 055501.
- 37 L. Wang, J. Zhao, F. Li and Z. Chen, *Chem. Phys. Lett.*, 2010, **501**, 16–19.
- 38 C. Adamo and V. Barone, *J. Chem. Phys.*, 1999, **110**, 6158–6170.
- 39 R. Krishnan, J. S. Binkley, R. Seeger and J. A. Pople, *J. Chem. Phys.*, 1980, **72**, 650–654.
- 40 M. J. Frisch, G. W. Trucks, H. B. Schlegel, G. E. Scuseria, M. A. Robb, J. R. Cheeseman, G. Scalmani, V. Barone, B. Mennucci and G. A. Petersson, *et al.*, Gaussian 09, Revision B. 01, Gaussian Inc., Wallingford, CT, 2010.
- 41 D. Feller, *J. Comput. Chem.*, 1996, **17**, 1571–1586.
- 42 K. L. Schuchardt, B. T. Didier, T. Elsethagen, L. Sun, V. Gurumoorthi, J. Chase, J. Li and T. L. Windus, *J. Chem. Inf. Model.*, 2007, **47**, 1045–1052.
- 43 J. Čížek, *Adv. Chem. Phys.*, 1969, **14**, 35–89.
- 44 G. D. Purvis III and R. J. Bartlett, *J. Chem. Phys.*, 1982, **76**, 1910–1918.
- 45 K. Raghavachari, G. W. Trucks, J. A. Pople and M. Head-Gordon, *Chem. Phys. Lett.*, 1989, **157**, 479–483.
- 46 (a) H. J. Werner, P. J. Knowles, G. Knizia, F. R. Manby, M. Schütz, P. Celani, T. Korona, R. Lindh, A. Mitrushenkov and G. Rauhut, *et al.*, MOLPRO, version 2012.1, see <http://www.molpro.net>; (b) H. J. Werner, P. J. Knowles, G. Knizia, F. R. Manby and M. Schütz, *WIREs Comput. Mol. Sci.*, 2012, **2**, 242–253.
- 47 J. V. Vondele, M. Krack, F. Mohamed, M. Parrinello, T. Chassaing and J. Hutter, *Comput. Phys. Commun.*, 2005, **167**, 103–128.
- 48 D. Yu. Zubarev and A. I. Boldyrev, *Phys. Chem. Chem. Phys.*, 2008, **10**, 5207–5217.
- 49 R. Bauernschmitt and R. Ahlrichs, *Chem. Phys. Lett.*, 1996, **256**, 454–464.
- 50 P. v. R. Schleyer and C. Maerker, *J. Am. Chem. Soc.*, 1996, **118**, 6317–6318.
- 51 G. J. Wang, M. F. Zhou, J. T. Goettel, G. J. Schrobilgen, J. Su, J. Li, T. Schlöder and S. Riedel, *Nature*, 2014, **514**, 475–477.
- 52 D. Ciuparu, R. F. Klie, Y. Zhu and L. Pfefferle, *J. Phys. Chem. B*, 2004, **108**, 3967–3969.